JOURNAL OF CATALYSIS **178,** 540–554 (1998)
ARTICLE NO. CA982175

A Theoretical Study of Carbon Chemisorption on Ni(111) and Co(0001) Surfaces

David J. Klinke II,* Steffen Wilke,† and Linda J. Broadbelt*,[1]

*Department of Chemical Engineering, Northwestern University, Evanston, Illinois 60208; and †Corporate Research, Exxon Research and Engineering Company, Annandale, New Jersey 08801

Received January 12, 1998; revised May 26, 1998; accepted June 1, 1998

Atomic carbon is a key intermediate which interacts with the surface during hydrocarbon growth reactions over transition metal surfaces. However, experimental data are scarce, available only for carbon–metal binding energies on nickel (111) and (100) single crystal surfaces. Therefore, to deepen our understanding of the chemisorption of carbon and to quantify its role in the catalytic formation of hydrocarbons, we have calculated the binding energy of atomic carbon on Ni(111) and Co(0001) surfaces using density-functional theory within the generalized gradient approximation and the full-potential linear augmented planewave (FP-LAPW) method. The results presented are in excellent agreement with known experimental values and substantially expand the database of geometric and energetic parameters describing adsorption of carbon on nickel and cobalt surfaces as a function of surface coverage and the adsorption site. The surface coverage dependence of the binding energy will be discussed and is used to interpret the tendency of the different surfaces toward molecular weight growth and their intrinsic reactivities.

1. INTRODUCTION

The search for improved catalysts and catalytic reaction conditions has been advanced significantly with the advent of microkinetic modeling (1), in which catalytic chemistry is examined in terms of elementary chemical reactions that occur on the catalytic surface. However, describing the chemistry at this level of detail presents a formidable challenge due to the number of thermodynamic and kinetic parameters which must be specified or estimated. Experimental data provide a rich source of these values but in many cases are not available. *Ab initio* level computational quantum chemical calculations provide a reliable and accurate alternative; however, the computational burden imposed by available techniques prohibits description of the reaction mechanisms composed of more than a small number of surface intermediates.

To address this challenge, we have developed a hierarchy for the specification of the parameters of microkinetic models to describe reactions involving metal surfaces which provides a reasonable compromise between accuracy and computational demand. The heart of the methodology is a phenomenological approach for the estimation of chemisorption energies of surface species (2). This approach relates the heat of chemisorption of species AB, where A interacts with the surface, to the atomic binding energy of A to the surface. Atomic binding energies may be obtained from experimental data, but in their absence, more rigorous *ab initio* quantum chemical techniques must be used due to the presence of the metal surface.

This hierarchical methodology for the construction of microkinetic models was applied to Fischer–Tropsch (FT) synthesis, a technology for the production of transportation fuels and chemicals from carbon monoxide and hydrogen. FT chemistry has received renewed attention as an environmentally attractive alternative to traditional refining processes. In the case of the hydrocarbon growth reactions comprising FT synthesis, atomic carbon is a key intermediate which interacts with the surface. However, experimental data are scarce, available only for carbon–metal binding energies on nickel (111) and (100) single crystal surfaces. Furthermore, the interpretation of these values is clouded by the disagreement in the literature as to the exact configuration of the adsorbed atomic carbon. Therefore, to deepen our understanding of the chemisorption of carbon and its role in the catalytic formation of hydrocarbons and to obtain the requisite model parameters, we have calculated the binding energy of atomic carbon on Ni(111) and Co(0001) surfaces using density-functional theory within the generalized gradient approximation (3) and the full-potential linear augmented planewave (FP-LAPW) method (4, 5).

Despite their close proximity in the periodic table, nickel and cobalt-based catalysts result in different product selectivities and reactivities, as shown in Table 1 for similar conditions. To probe the behavior of these two metals, the Co(0001) surface was selected as a prototypical Fischer–Tropsch catalyst, while the Ni(111) surface was chosen as a methanation catalyst. The differences in molecular weight growth chemistry for different transition metal

[1] Corresponding author. E-mail: broadbelt@nwu.edu.

0021-9517/98 $25.00

TABLE 1

Summary of Selectivity and Reactivity of Cobalt and Nickel Catalysts for Fischer–Tropsch Synthesis Reported by Vannice (40)

Catalyst	Temp (K)	H_2:CO	% Yield C_1	C_2	C_3	C_4	C_5	TON @ 548 K $\times 10^3$
2% Co/Al_2O_3	513	3.0	80.9	7.4	7.1	2.4	1.5	20
5% Ni/Al_2O_3	515	3.2	89.6	7.1	3.1	0.4	—	32

surfaces have been interpreted by many researchers, including van Santen *et al.* (6), who noted that chain growth is favored over methanation on metals which have a significant surface coverage of reactive carbon and with a long residence time for adsorbed CH_x intermediates. Furthermore, they point out that the hydrogenation steps for methane formation require that new hydrogen–carbon bonds replace the broken metal–carbon bonds, while formation of carbon–carbon bonds only requires the rupture of metal-Π-type bonds, which are less sensitive to valence–electron occupation than metal–carbon bond strengths. This implies that the activation energy for carbon–carbon bond formation will be less sensitive to valence–electron occupation changes than hydrogenation rates. In this work, we will further quantify this picture over Ni(111) and Co(0001) and show that both carbon–carbon bond formation and metal–carbon bond strengths are dependent on valence–electron occupation.

2. BACKGROUND

The majority of experimental investigations aimed at understanding the interaction of carbon with transition metal surfaces has been motivated by industrially important reactions such as methanation and Fischer–Tropsch synthesis. Different carbon phases have been detected on working catalysts, primarily nickel-based materials, and understanding their role in hydrocarbon synthesis has spawned numerous studies. For example, Goodman and co-workers identified two different carbon phases through Auger analysis of an active nickel catalyst after reaction at atmospheric pressure and 600 K (7–10). The two observed carbon phases were identified based on chemical reactivity, where the active carbon phase leading to hydrocarbon product formation was designated as the "carbidic" form and the inactive carbon phase producing catalyst deactivation was designated as the "graphitic" form.

These observations suggest that surface science investigations aimed at understanding the energetic basis for the different carbon surface phases by examining the energy of interaction of carbon with the surface would be valuable. However, experimental data for atomic carbon binding energies on single crystal surfaces are scarce. The only known data exist for Ni(100) and Ni(111) single crystal surfaces which were reported in a series of articles by Blakely and co-workers (11–14). In these studies, the heat of segregation to the surface of atomic carbon dissolved in bulk nickel was determined. The energy of adsorption was estimated through a thermodynamic cycle using the heats of vaporization, solution, and segregation.

The experimental studies by Blakely and co-workers (11–14) also examined variations in carbon coverage on nickel surfaces in detail. Isett and Blakely (12, 13) found for Ni(100) that the carbon coverage was directly related to the temperature and was well described by a Langmuir model, i.e., noninteracting localized segregated carbon atoms. They also reported that the variation of the total binding energy of a carbon atom to the Ni(100) surface in a coverage range of $0.3 \leq \Theta \leq 0.68$ was less than 2%. The lack of a surface coverage dependence of the binding energy reported by Blakely and co-workers has potentially led to misrepresentation of experimental results in which other researchers report isolated carbon–nickel binding energies using values derived from high surface coverage conditions (15). In contrast to the Ni(100) results, sharp changes in carbon coverage versus temperature were observed for Ni(111), indicating the presence of distinct surface carbon phases. In the high temperature phase, carbon existed as a combination of carbon as a bulk solution and possible isolated surface adatoms. Upon cooling to temperatures below approximately 1080 K, a phase transition occurred, and the carbon phase was identified as a monolayer of graphite. Therefore, the experimental value of the carbon binding energy to Ni(111) reported equal to 7.55 eV (11) refers to a monolayer of graphite. Although an isolated carbon adatom was not observed at lower temperatures, an estimated binding energy of $\leq$159.9 kcal/mol was reported (13). In addition, Isett and Blakely estimated the binding energy of carbon on Ni(111) in the fcc threefold hollow as 152.9 kcal/mol and in the hcp threefold hollow as 123.0 kcal/mol using a theoretical bond-energy bond-order model approach developed by Weinberg and Merrill (16, 17).

Although experimental investigations of carbon binding on nickel single crystals are limited, similar studies of carbon chemisorption on cobalt surfaces are even more scarce. One of the few examples was provided as a minor point by Eizenberg and Blakely (14) in their study of carbon on Ni(111). After reporting carbon phase condensation over Ni(111), they indicated that similar phase condensation behavior was observed over Co(0001). However, neither the nature of the carbon phase nor the possibility of its presence on other cobalt surfaces was probed through further experimentation.

In recent investigations, several groups of researchers have attempted to fill voids in the experimental investigations of carbon binding on nickel and cobalt by performing

TABLE 2

Summary of Carbon–Metal Binding Energies and Bond Lengths on Ni(111) and Co(0001) Surfaces Reported in the Literature

	ASED [23]		DFT [22]		Exp.	
Site	E_b [eV]	Å	E_b [eV]	Å	E_b [eV]	Å
Ni(111) graphite	—	—	—	—	7.55 [11]	1.42 [31], 2.16 [32]
Ni(111) top-on	8.38	2.20	3.92	1.66	—	—
Ni(111) bridge	8.38	1.95	4.93	1.77	—	—
Ni(111) fcc hollow	8.59	2.01	6.17	1.80	—	—
Ni(111) hcp hollow	8.74	2.01	—	—	—	—
Co(0001) top-on	—	—	5.12	1.60	—	—
Co(0001) bridge	—	—	5.69	1.76	—	—
Co(0001) fcc hollow	—	—	6.58	1.81	—	—
Co(0001) hcp hollow	—	—	—	—	—	—

theoretical studies. Varying combinations of effective medium theory and quantum mechanical calculations have been used by Darling *et al.* (18) and Nørskov and co-workers (e.g. (19)) and have resulted in the emergence of different carbon chemisorption pictures. Jacobsen *et al.* (19) predicted that carbon–metal densities were additive and as surface coverage increased, the height of the carbon above the surface increased to obtain the correct electron density, predicting a continuous evolution from isolated carbon atoms to a graphite overlayer. They also found that in a $p(1 \times 1)$ surface structure, carbon–carbon interactions were weak, and a coverage of two carbon atoms per surface metal atom was necessary to observe strong interactions. In contrast, Darling *et al.* (18) reported that as surface coverage increased, the carbon atoms were forced toward the metallic surface. The discrepancy between the decreasing carbon–metal distance as surface coverage increased and the large carbon–metal bond length found in the graphitic overlayer was attributed to the existence of a different mechanism whereby a nucleation step was required.

In an effort to reduce the computational demand imposed by more rigorous *ab initio* calculations of chemisorption energies on transition metal clusters, efforts have been made to reduce the cluster size (15, 20, 21). In such systems, an investigation of the binding energy dependence on surface coverage is impractical, since variations in binding energy as a function of cluster size are observed and the calculations are nonperiodic. Despite these shortcomings, recent theoretical studies carried out by the van Santen group help to elucidate the nature of carbon bonding on transition metals (22, 23).

The role of carbon in hydrocarbon synthesis reactions is further clouded by the possibility that subsurface carbon may be stable at reaction conditions, as suggested by the high temperature stability of bulk nickel carbide and experimental observations. Periodic trends for the stability of bulk and surface carbide layers were investigated by Joyner *et al.* (24). In addition, the role of subsurface carbon in Fischer–Tropsch synthesis over a nickel surface was investigated by Barbier and co-workers (25). Although analogous studies probing the role of cobalt carbide in hydrocarbon synthesis have not been carried out, periodic trends indicate that the stability of transition metal bulk carbides decreases on going to the right across the periodic table. This trend indicates that cobalt bulk carbide, Co_3C, should be slightly more stable than Ni_3C. One study which probed this stability was carried out by Zonnevylle *et al.* (26) who reported preliminary energetics for the conversion of a surface carbidic layer to subsurface carbon on a nine-atom Co(0001) cluster using a local density functional approach.

The quantitative results from the combined experimental and theoretical investigations reported in the literature of the binding of carbon to nickel and cobalt single crystal surfaces are summarized in Table 2. From the sparseness of this table, it is evident that there is a lack of sufficient data for the development of a clear picture of the nature of carbon binding to these materials. Insight into carbon chemisorption over nickel has been partially developed through the studies of Blakely and co-workers, but their work also underscores the difficulty in quantifying the binding of an isolated carbon atom on nickel surfaces through experiment. Despite its importance as a FT synthesis catalyst, even less is known about carbon chemisorption over cobalt. Various theoretical investigations have attempted to fill the gaps left by the experimental studies, but unfortunately most of the methods employed either lacked the complexity to describe chemisorption on transition metals quantitatively or to explore the surface coverage dependence of the chemisorption energy. Accurate quantitative values of adsorption energies as a function of surface coverage are a critical element in constructing a mechanistic description of FT synthesis kinetics. To address these needs, we have carried out a detailed theoretical investigation of the binding of carbon on Ni(111) and Co(0001) surfaces. By performing the calculations with periodic surface models, the adsorption position and the interatomic separation, i.e. surface coverage, were

explicitly specified and cluster effects were eliminated. The results obtained provide quantitative information about the energetic requirements for adsorption of carbon as a function of the surface coverage and mobility of carbon on the surface, and they allow us to begin to probe the differences in FT synthesis product selectivities for these two distinct surfaces.

3. METHOD

The full-potential linear augmented planewave (FP-LAPW) method provides tremendous promise for accurate calculation of chemisorption energies as compared to conventional wave-function-based and semi-empirical methods. The chief advantage of the FP-LAPW method as applied to surface chemistry is the simulation of the extended surface, such that calculations are not limited by the cluster approximation, and the surface coverage dependence of chemisorption energies can be explored. In addition, the FP-LAPW method employs an unbiased basis set, enabling an equal description of localized molecular and extended metal states.

The primary aim of this work was to obtain a reliable estimate of the chemisorption energies of carbon on Ni(111) and Co(0001) within a designed accuracy of 200 meV. Although extrapolation to real catalyst systems may be further complicated by surface nonuniformity due to the presence of edges, defect sites, support contributions, and additional coadsorbates, the first step in understanding the interaction of carbon with these catalysts was to probe ideal surfaces. Specifically, the interaction of carbon with the most important high symmetry adsorption sites was examined.

All of the calculations were performed using density functional theory within the generalized gradient approximation (GGA) and the FP-LAPW method. The GGA represents the most serious approximation in the calculations concerning the overall accuracy. The GGA has been found to reproduce energies and geometries with an accuracy comparable to the MP2 approximation known from quantum chemistry (3). The FP-LAPW wave functions were represented in the interstitial region using a plane-wave expansion up to $E_{\text{cut}} = 15$ *Ry* and for the potential representation plane waves up to $E_{\text{cut}} = 169$ *Ry* were used. Inside the muffin-tin spheres, the wave functions were expanded in spherical harmonics with $l_{\max} = 10$, and the nonspherical components of the density and potential were included up to $l_{\max} = 4$. For the *k* integration, at least 150 uniformly spaced points in the two-dimensional Brillouin zone corresponding to the hexagonal (1×1) surface unit cell were used. All calculations were performed nonrelativistically and nonspin-polarized. A spin-polarized calculated binding energy was compared to a nonspin-polarized binding energy, and the difference was less than 100 meV. However, given the numerical accuracy required to provide a valid comparison among binding energies, the difference was not significant enough to change the overall energetic picture. Therefore, nonspin-polarized calculations were performed to reduce the overall computational burden by 50%.

To achieve a balance between computational tractability and a realistic representation of the catalyst surface, a supercell geometry was used. The metal substrate was represented by a five-layer slab for nickel and a six-layer slab for cobalt separated by a 10-Å thick vacuum region. Carbon atoms were placed on both sides of the slab surface, which was periodic in two dimensions. The surface unit cell contained one to four metal atoms, depending on the surface coverage being investigated. The carbon adsorption height and interplanar spacings were allowed to relax, while other atomic parameters were fixed to maintain a high degree of symmetry in the calculations. Although surface reconstruction has been observed for carbon chemisorbed on the Ni(111) surface at surface coverages greater than 0.45 ML (27), Klink *et al.* suggest that the surface reconstruction is caused by a carbon atom located in a subsurface site. Accommodating carbon atoms in the subsurface would require significant interplanar relaxation, which is the effect modeled in our work. The energetic difference for intraplanar geometry relaxation of the metal–metal bonds of the surface reported by Zonnevylle and co-workers (26) was small, i.e., approximately 0.1 eV. Therefore, neglecting intraplanar relaxation to reduce the computational demand should not significantly change the overall energetic picture obtained. The convergence was tested using a plane-wave cutoff for the wave-function expansion of $E_{\text{cut}} = 13.32$ *Ry* against a higher plane-wave cutoff of $E_{\text{cut}} = 15.0$ *Ry*. The resulting changes of the binding energy were found to be less than 120 meV. The slab model assumption was tested by increasing the number of metal layers to seven, and the binding energy changed by less than 100 meV.

The binding energy of a carbon atom as it is referred to throughout the paper is defined as the DFT-GGA total energy. From the total energy of the free carbon atom, E_{C}, and the total energies per unit cell of the clean surface, E_{M}, and carbon-covered slabs at different surface coverages, $E_{M:\text{C}}(\Theta)$ ($M = \text{Ni, Co}$), the binding energy per carbon atom as a function of surface coverage, $E_{\text{b}}(\Theta)$, was calculated as shown in Equation [1],

$$E_{\text{b}}(\Theta) = -1/N_{\text{C}}[E_{M:\text{C}}(\Theta) - E_M - N_{\text{C}}E_{\text{C}}], \qquad [1]$$

where N_{C} is equal to the number of carbon atoms per unit cell. The zero energy of a spin-polarized isolated carbon atom, E_{C}, was obtained with the same parameters used in the $E_{M:\text{C}}$ calculation.

The electronic changes upon chemisorption of both the adsorbate and the transition metal surface were represented by the density of states (DOS) plots projected onto particular orbitals inside the muffin-tin sphere of the atoms comprising the unit cell. The concept of projected DOS has

been shown to be a useful tool to interpret the changes in the electronic structure upon chemisorption through application of simple models of chemical reactivity and bonding (28, 29).

4. RESULTS

4.1. Bulk Nickel and Nickel(111) Surface

The lattice parameters used in all calculations were first calculated using a fcc bulk metal crystal. The bulk nickel lattice parameter was obtained using both spin-polarized and nonspin-polarized calculations. For spin-polarized calculations, lattice parameters of 6.678 and 6.700 a.u. were obtained using a planewave energy cutoff of 13.32 and 16.0 *Ry*, respectively. For nonspin-polarized calculations, lattice parameters of 6.664 and 6.674 a.u. were obtained. These values were consistent with the experimental value of 6.658 a.u. (30). The clean Ni(111) surface showed a slight inward relaxation of the topmost Ni layer by -1.5% of the bulk interlayer distance, d_o. The calculated work function of 5.15 eV was comparable to the reported value of 5.35 eV (31).

4.2. Adsorbed Carbon on Ni(111)

In order to probe the dependence of the binding energy on surface coverage, the number of carbon atoms per unit cell was varied. The different monolayer (ML) coverages were modeled by one carbon atom per hexagonal (1×1) unit cell for 1 ML, (2×1) unit cell for 0.5 ML, and (2×2) unit cell for 0.25 ML. The subsurface position was modeled by switching the position of the fcc hollow carbon overlayer with the top metal layer. In this work, the coverage is defined as the number of carbon atoms per 1×1 hexagonal surface cell.

The binding energy of all possible high symmetry adsorption sites was calculated to determine the most energetically favorable site. The calculated values of the binding energy, the adatom–metal bond length, the top-layer relaxation, and the work function change as a function of surface coverage and adsorption site are summarized in Table 3. As shown in Table 3, the fcc hollow is the most energetically favorable position for carbon chemisorption on Ni(111) at all coverages. The relative stabilities are described as follows: fcc hollow $\simeq$ hcp hollow $\gg$ bridge $\gg$ top-on site.

Density of states plots provided insight into the character of the chemisorbed carbon as a function of surface coverage. The layer and orbital resolved density of states for carbon adsorbed in the fcc hollow sites with a coverage of $\Theta = 0.25$ and $\Theta = 1.0$ are shown in Fig. 1. For the surface and subsurface nickel layers, the dashed line reveals the contribution of the Ni(4s + p) orbital and the solid line denotes the Ni(3d) orbital contribution to the density of states. The most striking characteristic of the bonding is the formation of a C(2s) band approximately 11 eV below the Fermi level. For $\Theta = 0.25$, this C(2s) band is very sharp and does not interact with the broad nickel d-band. The shape of the C(2s) band indicates isolated carbon–metal bonding. At 1 ML coverage, the band is broad; this breadth is due to direct carbon–carbon interactions on the surface rather than indirect interactions through the metal surface.

TABLE 3

Calculated Values of Binding Energy, E_b; Adatom–Metal Bond Length, R; Top-Layer Relaxation, Δd_{12}; and Work Function Change, $\Delta\Phi$, for Carbon on the Ni(111) Surface

Coverage Θ	Site	E_b [eV]	R [Å]	Δd_{12} $\%d_o$	$\Delta\Phi$ [eV]
2	graphite	7.65	1.44[a], 2.11[b]	+0.5	−1.549
1	top-on	4.38	1.76	+10.4	+1.537
1	bridge	4.65	1.87	+9.6	+1.792
1	fcc hollow	4.97	1.89	+8.8	+1.551
1	hcp hollow	4.97	1.90	+8.6	+1.582
1	subsurface	6.16	1.91[c], 1.92[d]	+23.5	−0.377
0.5	fcc hollow	5.99	1.81	+6.0	+0.814
0.25	bridge	5.99	1.75	+7.1	+0.721
0.25	fcc hollow	6.68	1.79	+2.5	+0.643
0.25	hcp hollow	5.97	1.89	+6.5	+1.537
0.25	subsurface	7.30	1.85[c], 1.87[d]	+12.9	+0.018

[a] Graphitic carbon–carbon bond distance.
[b] Distance between top-on carbon and metal atom.
[c] Distance between adatom and top metal layer.
[d] Distance between adatom and middle metal layer.

The DOS plots in Fig. 1 provide additional insight into the nature of the metal–carbon bonding as a function of surface coverage. In the case of strong molecular bonding, the formation of distinct bonding states below the Fermi level and unoccupied antibonding states above the Fermi level is expected. When bonding occurs with a transition metal surface, the interaction of the wide *d*-bands with these states results in the formation of adsorbate bonding and antibonding bands. Strong molecular bonding is therefore evident in the 0.25-ML case, where the $C(2p_{x+y})$ and $C(2p_z)$ bonding bands are observed at -4.0 eV and the antibonding bands are in the range of 0.5–4.0 eV. Furthermore, bands observed at -11.0 eV for the $C(2p_z)$, C(2s), and Ni orbitals indicate a C(s + p) hybridization formed by interaction with the surface. In contrast, the results from the 1.0-ML case reveal the weakening of the bonds as the surface coverage increases, as captured by the increase in the DOS at the Fermi level. This increase in the DOS at the Fermi level for the $C(2p_z)$ orbital is caused by the formation of a new, partially nonbonding orbital. In addition, $C(2p_{x+y})$ antibonding states are slightly occupied right at the Fermi level. Therefore as surface coverage is decreased, the upward energy shift of the $C(2p_{x+y})$ orbitals, along with the creation of distinct bonding and antibonding $C(2p_z)$ orbitals, suggests that the carbon–nickel bond is rehybridized to include a $C(2p_z)$ contribution. However, the largest change for $\Theta = 0.25$ was

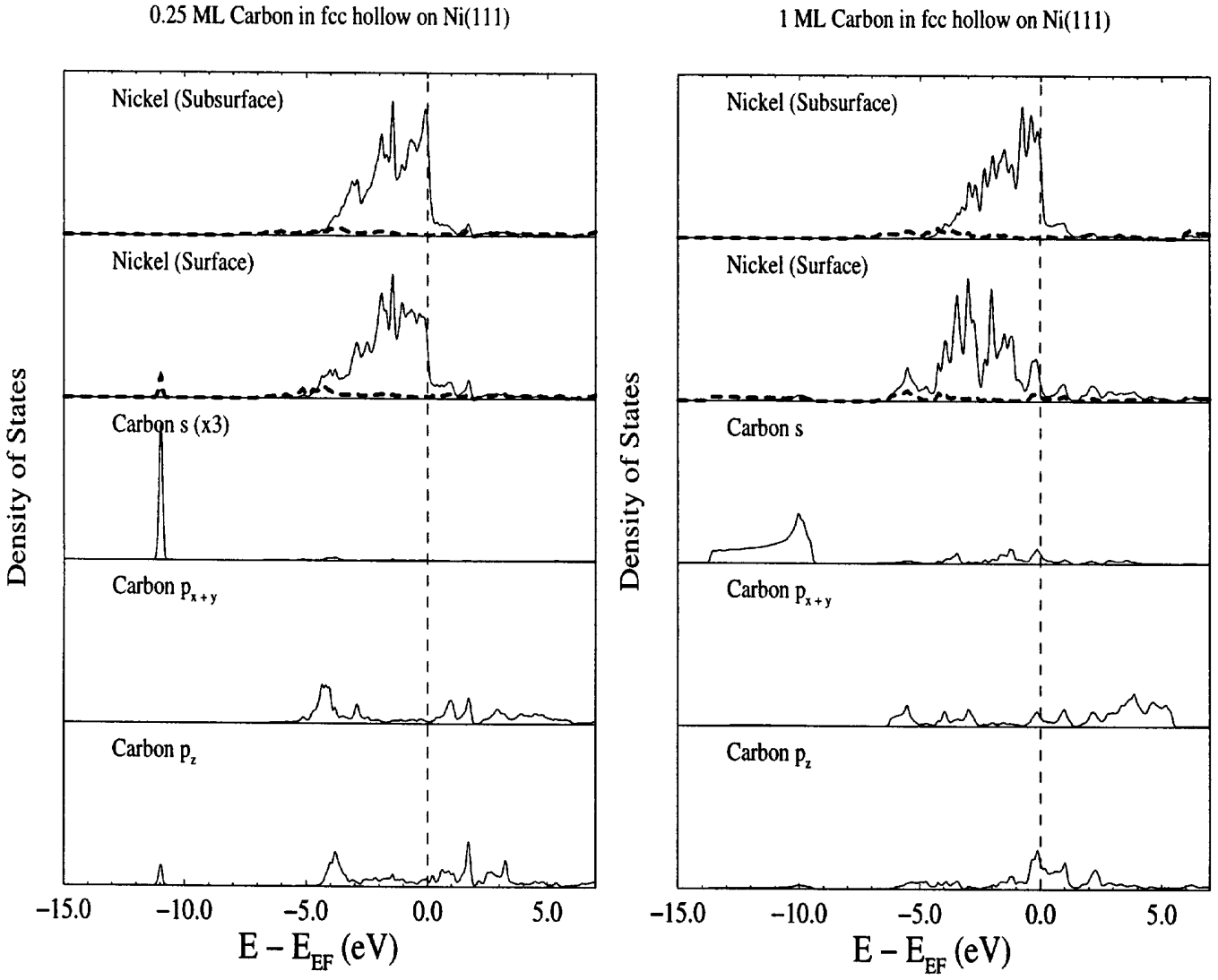

FIG. 1. Layer resolved density of states for 0.25 (left panel) and 1.0 ML (right panel) carbon on the Ni(111) surface at fcc three-fold hollow sites. The nickel 4(s + p) and 3d orbital contributions are represented by a dashed line and solid line, respectively.

observed for the decrease in energy relative to the Fermi level of the C(2s)-Ni(3d, 4s + p) interaction and the formation of bonding C($2p_z$)–Ni(3d, 4s + p) bands. This would explain the increase in binding energy at lower coverages despite the shifting of the center of the C($2p_{x+y}$) − Ni(3d, 4s + p) bands to higher energies relative to the 1-ML case.

At all surface coverages less than 1 ML, the changes in the nickel DOS introduced by the adsorbed carbon are largely confined to the surface layer. A 1-ML coverage, the surface DOS is severely affected, and as a result, the subsurface is modified by a slight reduction of the density of states in a region just below the Fermi level. Due to the high degree of bonding of the surface nickel atoms to carbon, the coordination to the subsurface atoms is decreased as observed by the slight upward shift of the center of the subsurface d-band to −1.111 eV and the increase in interplanar spacing observed in Table 3. Correspondingly, the surface metal d-band is narrowed and suggests the formation of a nickel–carbon alloy.

The electronic changes induced upon chemisorption of carbon atoms, relative to free carbon and the clean Ni(111) surface, are reflected in the density difference contour plots as a function of surface coverage shown in Fig. 2. The density difference plot graphically illustrates the spatial changes in electron density of both the carbon and metal surface upon adsorption. These results are presented in terms of a contour plot, where the plane chosen best represents the changes to both the carbon and metal atoms. Specifically, the electron density difference plots are shown for the chemisorption of carbon on the Ni(111) surface along

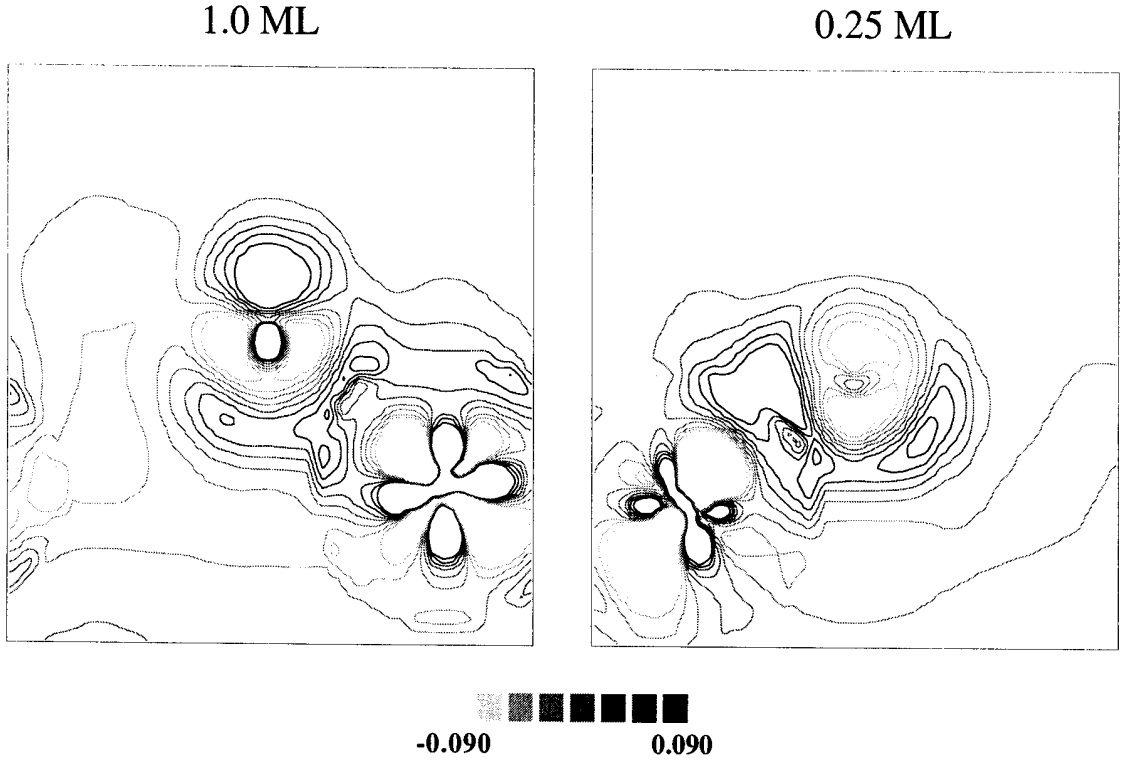

FIG. 2. Density difference plot for 1.0- and 0.25-ML carbon on the Co(0001) surface at hcp threefold hollow sites. The density difference is expressed in e/A^3.

an axis perpendicular to the surface plane in the (120) direction, relative to a hexagonal unit cell and bisecting a carbon atom and a nickel atom.

The density difference plots presented in Fig. 2 help to illustrate the changes in the character of the $C(2p_z)$ orbital as surface coverage is increased as noted above. As the coverage of carbon on the surface is increased, the charge on the surface is also increased, resulting in a repulsion. To relieve the repulsion, the carbon atoms form a $C(2p_z)$-C(2s) hybrid orbital to transfer the charge away from the surface, as shown by an increase in the charge in the lobe above the surface. Since this highly occupied lobe cannot take part in surface bonding, it is therefore at least partially nonbonding. The nonbonding dangling $C(2p_z)$ orbital revealed in the DOS plots of Fig. 1 is clearly observed for $\Theta = 1.0$ above the carbon atom and extending outward from the surface.

Changes in the hybridization of the top-layer metal $Ni(3d_{z^2})$ orbital are also evident from the density difference contour plots of Fig. 2. Since each metal atom is bonding with three neighboring carbon atoms, the hybridization is in the three different directions. In the 0.25-ML case, the metal atom is bonded to only one carbon atom, and the depopulation of the $Ni(3d_{z^2})$ orbital is directed solely towards the carbon shown, indicating a localized bond. The rotation of the d_{z^2} orbital in the direction of the chemisorbed carbon atom is also observed.

The electronic and energetic picture obtained from these results is consistent with an increased reactivity of adsorbed carbon atoms as surface coverage increases to 1.0 ML. For an adsorbate interacting with a surface in a threefold hollow site, it is expected, in general, that at least sp^2 hybridization accounts for the surface bonding. In this work, it is observed that as surface coverage is increased, the hybridization shifts from sp^3 to sp^2, partially due to the formation of the nonbonding dangling $C(2p_z)$ orbital. This change in hybridization results in a corresponding decrease in the chemisorption energy, which in turn leads to an increase in the reactivity of the carbon atom as coverage increases.

To simulate subsurface carbon, a layer of carbon was located in the octahedral sites of the bulk nickel. As indicated by the values reported in Table 3, this subsurface adsorption energy was substantially greater than the most stable surface sites, the threefold hollow sites. At both $\Theta = 1.0$ ML and $\Theta = 0.25$ ML, reconstruction of the Ni(111) surface was suggested by the large surface relaxation, and the work function of the metal decreased substantially. In fact, the work function even changed sign for a coverage of one monolayer. The layer and orbital resolved density of states for carbon adsorbed in subsurface sites with a coverage of $\Theta = 0.25$ and $\Theta = 1.0$ are shown in Fig. 3. The stability of the subsurface carbon can be attributed to the formation of bonding $C(2p_z)-Ni(3d, 4s + p)$ orbitals which remain

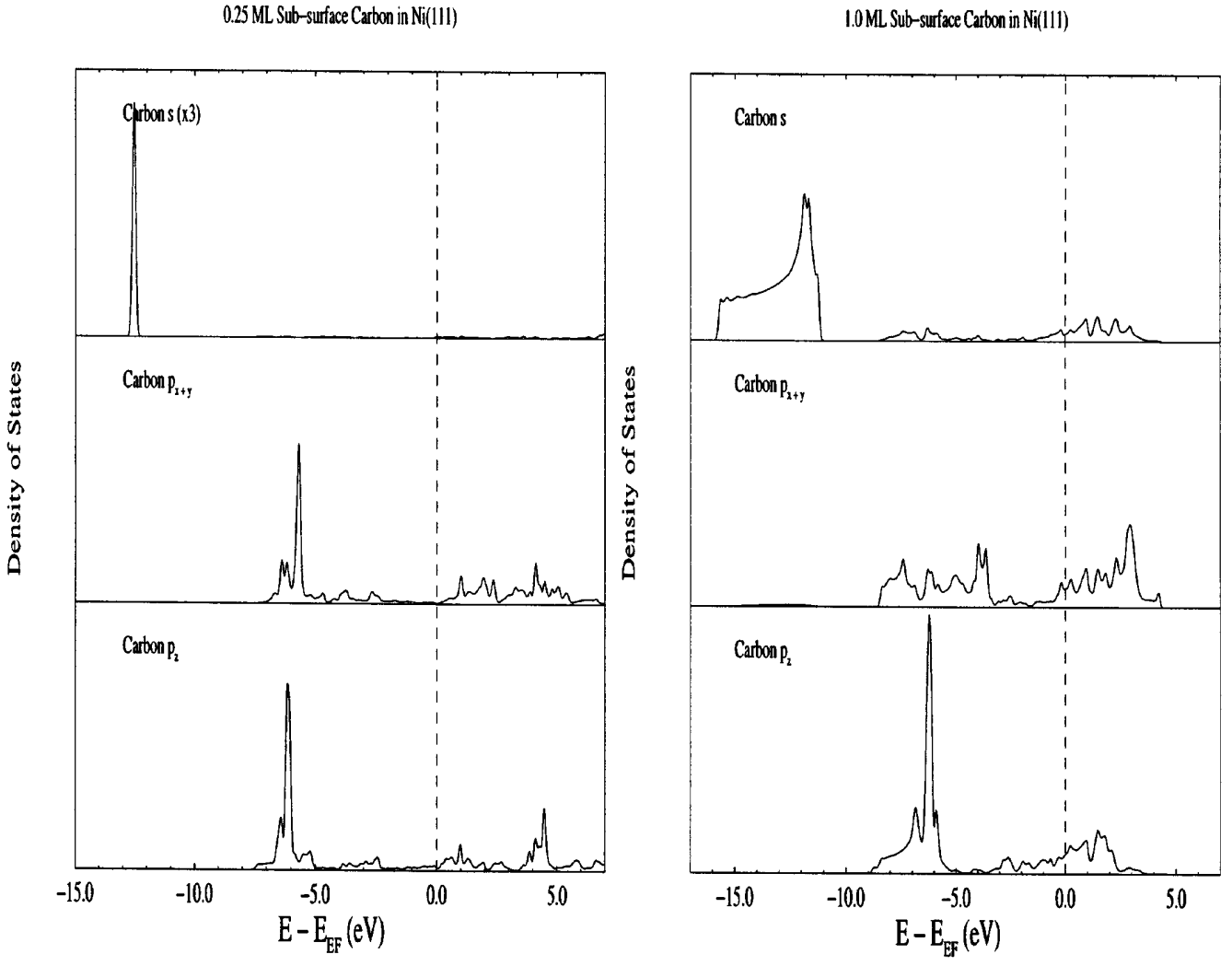

FIG. 3. Layer-resolved density of states for 0.25- (left panel) and 1.0-ML (right panel) subsurface carbon on the Ni(111) surface.

relatively unchanged as a function of surface coverage. In addition, the center of the bonding carbon p-states for the subsurface site is shifted to −6.0 eV relative to −4.5 eV for the surface hollow sites. The dependence to the character of the C(2s) and C($2p_{x+y}$) orbitals on surface coverage was similar to that observed for the surface sites. The broad band of the C(2s) orbital is again attributed to carbon–carbon interactions in the subsurface in the 1.0-ML case while in the 0.25-ML case the C($2p_{x+y}$) orbitals are localized. The split between bonding and antibonding C($2p_{x+y}$) orbitals is also increased in the 0.25-ML case.

4.3. Adsorbed Graphite on Ni(111)

The monolayer graphite surface was modeled by two carbon atoms per hexagonal (1 × 1) unit cell, one located in a fcc threefold hollow and one occupying a top-on site. This structure was selected based on the recent experimental results obtained from LEED intensity analysis of Gamo and co-workers (32). The calculated geometries reported in Table 3 were consistent with their results, where they found $\Delta d_{12} = 3.4\%$, a C_{top-on}-Ni distance equal to 2.16 Å, and an interplanar distance between carbon in the fcc hollow and nickel layer equal to 2.11 Å (32).

The DOS for free graphite and adsorbed graphite on Ni(111), shown in Fig. 4, reveals that the majority of the binding of carbon atoms is carbon–carbon bonding, as opposed to bonding of carbon to the nickel surface, and this character is unchanged upon adsorption. The main interaction of graphite with the surface is manifested through the DOS peak of the C($2p_z$) orbital of the top-on carbon around the Fermi level and broadening of both C($2p_z$) orbitals. The numerical values for the carbon-binding energy are consistent with the picture provided by the DOS. The binding energy of carbon in a free monolayer of graphite is 7.57 eV, and upon surface adsorption, the graphite monolayer is stabilized by the surface by only an additional 0.08 eV,

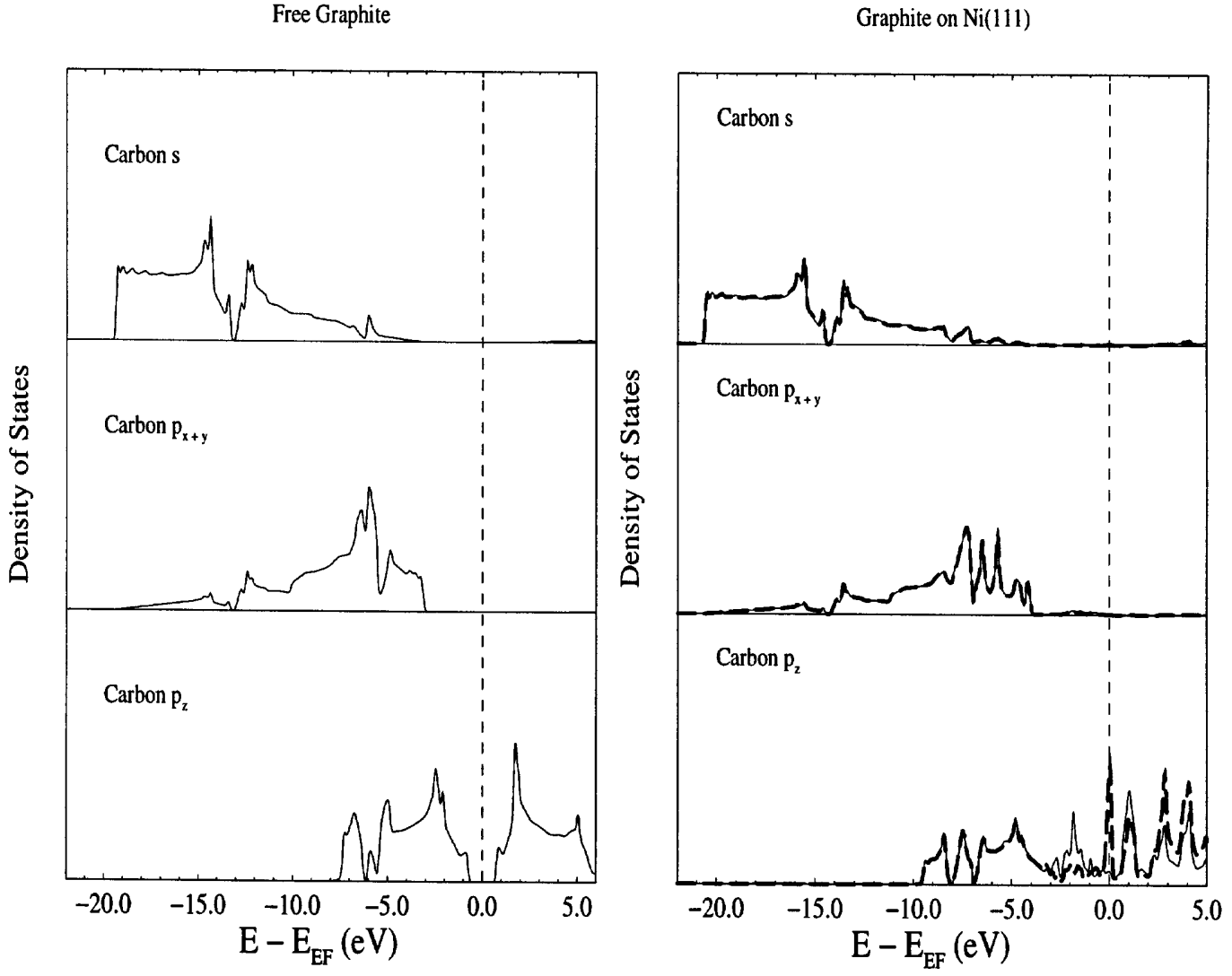

FIG. 4. Surface-resolved density of states for free graphite (left panel) and graphite monolayer (right panel) on a Ni(111) surface. The free graphite was represented by absorbed graphite on a Ni(111) structure without the Ni(111) surface present. In the free graphite DOS, both carbon atoms are identical while in the adsorbed graphite DOS; the top-on carbon is represented by a dashed line while the threefold hollow carbon is represented by a solid line.

resulting in a carbon binding energy of 7.65 eV. This result agrees quite well with the experimental results of Blakely *et al.* who reported the difference between free graphite and adsorbed monolayer graphite as 0.06 eV (11). The calculated $\Delta\Phi$ is also consistent with experiment, in which a value of -1.0 eV was reported by Rosei and co-workers (33).

4.4. Bulk Cobalt and Cobalt (0001) Surface

The same approach used to study the Ni(111) surface was employed to investigate the binding of carbon to a Co(0001) surface. Lattice parameters for subsequent Co(0001) calculations were first determined using an hcp bulk metal crystal. In this case, lattice parameters were only determined using nonspin-polarized calculations and a planewave energy cutoff of 16.0 *Ry*. The values obtained were equal to 4.669 and 7.540 a.u., which were in good agreement with the experimental values of 4.738 and 7.690 a.u. (30). It is important to note that accounting for spin-polarization will increase the lattice parameters due to magnetic pressure as seen in the bulk nickel calculations. The clean Co(0001) surface showed a slight inward relaxation of the topmost Co layer of -2.0%, relative to the bulk interlayer distance, d_o, and a work function of 5.18 eV was calculated.

4.5. Adsorbed Carbon and Graphite on Co(0001)

Using the same strategy employed for the Ni(111) surface, the binding energy of all possible high symmetry

TABLE 4

Calculated Values of Binding Energy, E_b; Adatom–Metal Bond Length, R; Top-Layer Relaxation, Δd_{12}; and Work Function Change, $\Delta\Phi$, for Carbon on the Co(0001) Surface

Coverage Θ	Site	E_b [eV]	R [Å]	Δd_{12} %d_o	$\Delta\Phi$ [eV]
2	Graphite	7.68	1.43[a], 2.11[b]	+2.0	−1.856
1	Top-on	4.61	1.70	+13.4	+1.591
1	Bridge	5.07	1.82	+12.5	+1.627
1	Fcc hollow	5.43	1.85	+12.8	+1.116
1	Hcp hollow	5.49	1.84	+11.9	+0.854
1	Subsurface	6.79	1.89[c], 1.92[d]	+26.7	−0.117
0.25	Bridge	6.21	1.75	+4.8	+0.747
0.25	Fcc hollow	6.88	1.80	+2.5	+0.714
0.25	Hcp hollow	7.05	1.79	+0.9	+0.636
0.25	Subsurface	6.72	1.82[c], 1.87[d]	+15.9	+0.076

[a] Graphitic carbon–carbon bond distance.
[b] Distance between top-on carbon and metal atom.
[c] Distance between adatom and top metal layer.
[d] Distance between adatom and middle metal layer.

adsorption sites was calculated to determine the most energetically favorable site on Co(0001). The calculated values of the binding energy, the adatom–metal bond length, the top-layer relaxation, and the work function change as a function of surface coverage and adsorption site are summarized in Table 4. In contrast to the Ni(111) results, the hcp hollow is the most energetically favorable surface site on Co(0001). The relative stabilities of isolated carbon atoms ($\Theta \leq 1.0$) are described as follows: hcp hollow > fcc hollow ≫ bridge ≫ top-on site. The calculated carbon–cobalt bond lengths are comparable to the experimental value of 1.75 ± 0.05 Å reported by Atrei *et al.* (34). Although the experimental accuracy of work function measurements is ±0.10 eV (35), the calculated results are in only qualitative agreement with a $\Delta\Phi = +0.30$ eV reported by Atrei and co-workers upon carbon chemisorption. Although the experimental database available for cobalt is limited, the small number of comparisons which can be made between experiment and the calculations reported in this work are in good qualitative and quantitative agreement.

The layer and orbital resolved density of states for carbon adsorbed in the hcp hollow sites of Co(0001) with a coverage of $\Theta = 0.25$ and $\Theta = 1.0$ are shown in Fig. 5. Direct comparison of these DOS plots and with those for Ni(111) in Fig. 3 provides a striking contrast between the characteristics of the carbon 2p orbitals as a function of surface coverage and the identity of the surface. As was observed for Ni(111), the bonding and antibonding C(2p) states observed at $\Theta = 0.25$ rehybridize at higher coverages, as demonstrated by the 1.0-ML case, forming a nonbonding, dangling C($2p_z$) orbital at the Fermi level, while the C($2p_{x+y}$) orbital band shifts to a lower energy. However, since nickel has one more 3d electron than cobalt, the Fermi level of cobalt is slightly lower, relative to the center of this nonbonding C($2p_z$) orbital and the bottom of the C($2p_{x+y}$) antibonding states, leading to a depopulation of these orbitals relative to Ni(111). The depopulation of these orbitals results in a lower surface coverage dependence of the carbon chemisorption energy. The DOS plots for adsorbed graphite and subsurface carbon on the Co(0001) surface are both similar to the results for Ni(111) and are therefore omitted.

Using the same orientation presented to examine carbon adsorption on Ni(111), the electronic changes induced upon chemisorption of carbon atoms, relative to free carbon and the clean Co(0001) surface, are reflected in the density difference contour plots as a function of surface coverage shown in Fig. 6. Specifically, the electron density difference plots are shown for the chemisorption of carbon on the Co(0001) surface along an axis perpendicular to the surface plane in the (120) direction, relative to a hexagonal unit cell and bisecting a carbon atom and a cobalt atom. The density difference results resemble those for carbon on Ni(111), as the nonbonding dangling C($2p_z$) orbital revealed in the DOS plots of Fig. 5 is also clearly observed for $\Theta = 1.0$ above the carbon atom extending outward from the Co(0001) surface. In contrast to the Ni(111) results, the C($2p_z$) orbital showed a slightly smaller charge accumulation. This is consistent with the DOS plot, where the nonbonding dangling C($2p_z$) orbital lay at a slightly higher energy and was slightly depopulated relative to the case for nickel. Changes in the hybridization of the top-layer metal Co($3d_{z^2}$) orbital are also evident.

5. DISCUSSION

The results obtained for the geometries and energies of carbon adsorption on Ni(111) as a function of the adsorption site are consistent with standard theories of chemisorption. As expected, the most stable adsorption site on Ni(111) was the fcc threefold hollow at all surface coverages. The carbon–metal atomic distances reported in Table 3 decreased as the coordination of the carbon atom with the metal increased, consistent with the reported increase in the carbon–metal bond strength (36). Furthermore, carbon adsorbed in the subsurface had the highest binding energy for all coverages less than the graphite structure, consistent with the high coordination of carbon with metal atoms. In addition, the large surface relaxation values obtained for carbon in subsurface positions suggest probable surface reconstruction as observed experimentally for the Ni(111) surface (27).

One of the most striking results of this work, presented in Fig. 7, is the dependence of the binding energy of the most stable adsorption configuration on surface coverage. Because it is difficult to probe experimentally the dependence of binding energy on the surface coverage and the site of

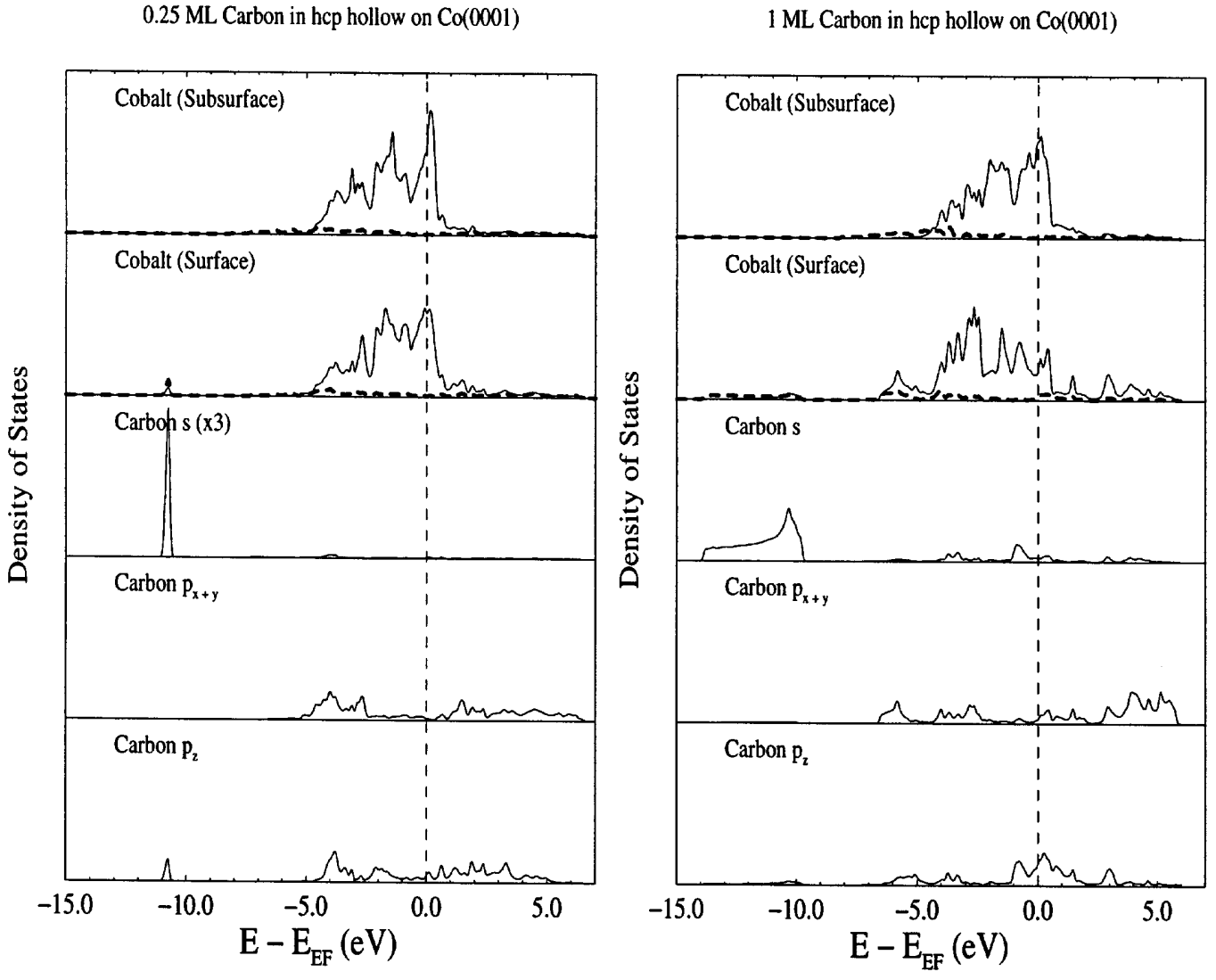

FIG. 5. Surface resolved density of states for 0.25- (left panel) and 1.0-ML (right panel) carbon on the Co(0001) surface at hcp threefold hollow sites. The cobalt 4(s + p) and 3d orbital contributions are represented by a dashed line and a solid line, respectively.

interaction simultaneously, the calculations reported here provide the most comprehensive investigation of the interplay of these two variables. Specifically, the difference of the adsorption energy between the fcc and hcp threefold hollow sites at 1-ML coverage is insignificant, while the differences between either of the threefold hollow sites and the other adsorption sites on the surface were greater than 0.32 eV for Ni(111).

These results may be used as an indication of the surface diffusion barriers for carbon migration on Ni(111) and Co(0001) surfaces. The change in binding energies at different sites relative to the binding energy for an fcc hollow site is shown for coverages of 0.25 ML and 1.0 ML in Fig. 8. The differences in binding energy among the different surface sites increased as the surface coverage decreased; for example, over Ni(111) ΔE_b (*fcc hollow − bridge*) was equal to 0.71 eV for the lowest coverage studied as compared to the value of 0.32 eV for 1-ML coverage. If the change in energy between two stable surface sites is used as a measure of the activation energy required for movement between these sites, this suggests that surface migration is more difficult for an isolated carbon atom than for a carbon sitting on a crowded surface. These values also suggest that surface migration is more difficult over cobalt than over nickel, and the difference between these catalysts is dependent on the surface coverage. The facile surface migration at 1.0 ML also provides low energy pathways for conversion to the more stable carbon configurations indicated in Fig. 7, i.e. isolated carbon and graphitic carbon, which are both over 1.5 eV more stable than 1.0 ML.

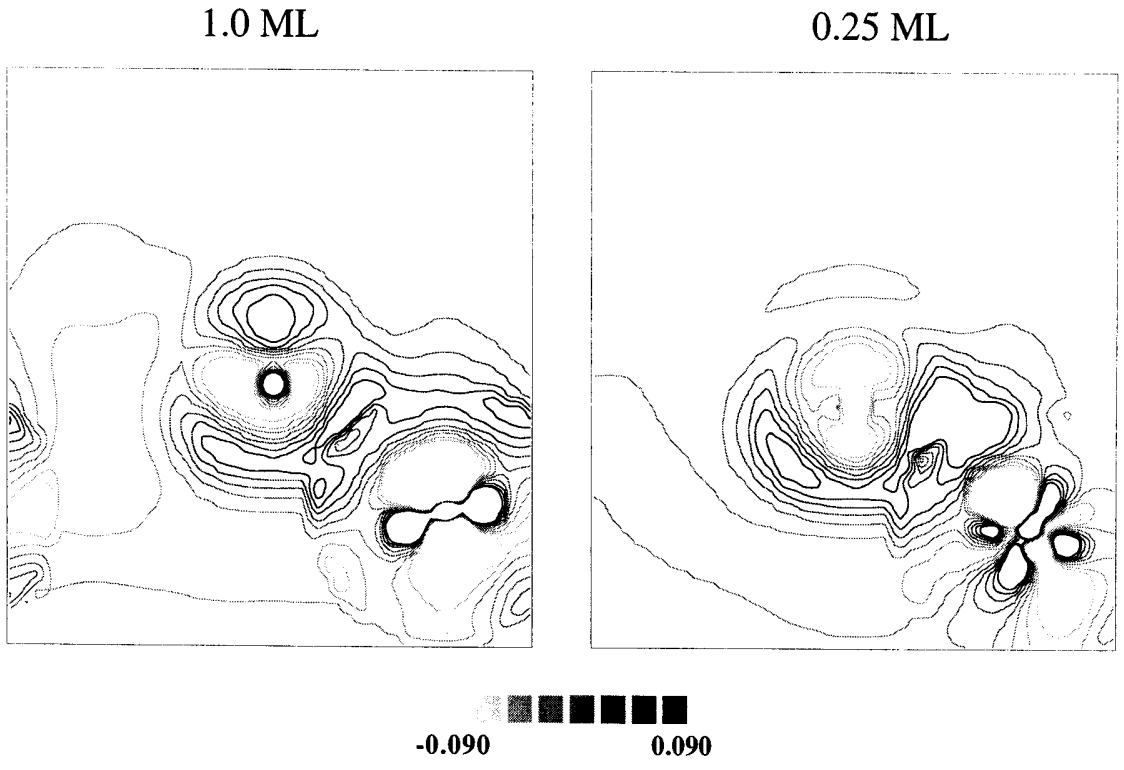

FIG. 6. Density difference plot for 1.0- and 0.25-ML carbon on the Co(0001) surface at hcp threefold hollow sites. The density difference is expressed in e/A^3.

The characteristics and energetics of a graphitic monolayer on Ni(111) calculated in this work were also consistent with further experimental information. The configuration for graphite suggested by Gamo and co-workers and used in these calculations, in which carbon occupies both fcc threefold hollow sites and on-top sites, is consistent with the STM results, where only the top-on atoms would be observed. STM provides a spatially resolved density of electrons with energies close to the Fermi level. Therefore, a large DOS at the Fermi level will result in a larger current. As shown in the DOS projected onto the distinct carbon atoms, the carbons occupying top-on sites have a large peak right at the Fermi level which may induce electronic effects that increase the tunneling current observed by STM. Rosei *et al.* (33) reported that the interaction of a graphite monolayer with the Ni(111) surface caused a shift of the major features of the carbon–carbon bonding orbitals by only 1 eV. This is in excellent agreement with the results of the calculations that revealed that the density of states between free graphite and graphite on Ni(111) system decreased by 1 eV. In addition, the orbital interactions reported herein are consistent with the suggestions of Gamo and co-workers, who indicate that there is not much overlap between π carbon orbitals and the metal surface orbitals. As shown in our calculations and observed experimentally (37), the greatest interaction of carbon with the surface is through the top-on adsorbates and nickel at the Fermi level.

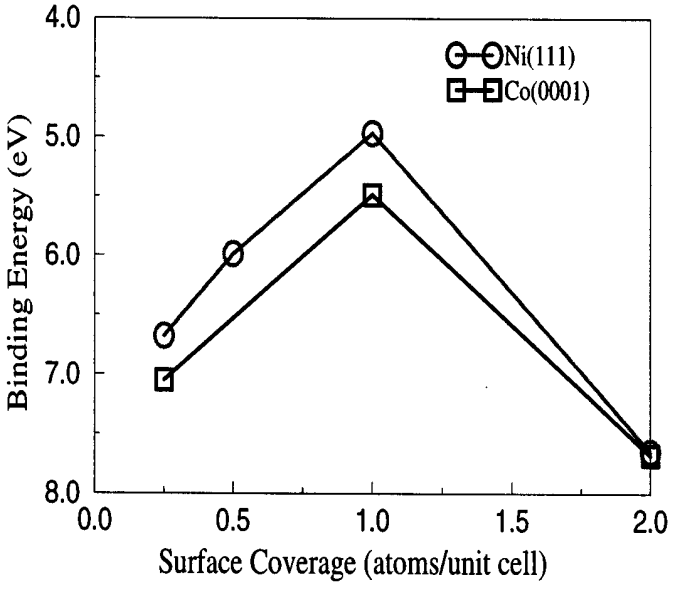

FIG. 7. Surface coverage dependence of carbon binding energy on Ni(111) and Co(0001) surfaces.

The changes in the characteristics of the Ni(111) and Co(0001) surfaces as a function of surface coverage can be further quantified through the calculated values of the work

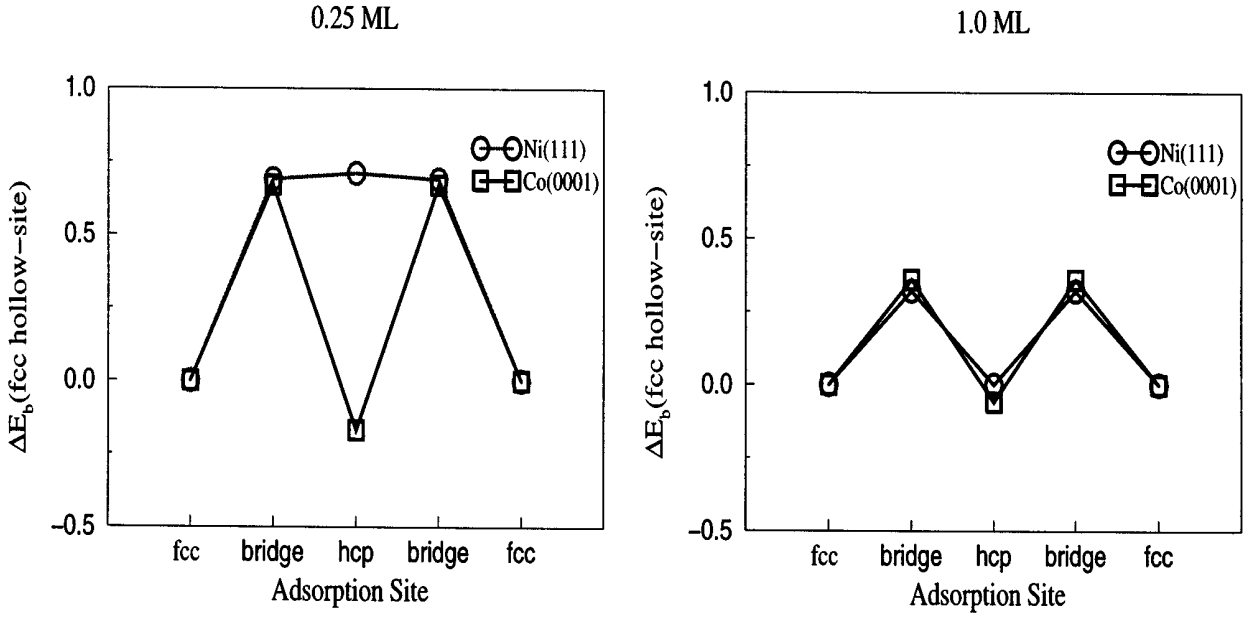

FIG. 8. Difference in carbon-binding energy on nickel and cobalt as a function of the adsorption site for $\Theta = 0.25$ (left panel) and 1.0 (right panel).

function. The work function is defined as the energy required to remove an electron from the surface, and changes in the work function upon adsorption indicate the nature of the electronic interaction between the adsorbate and the surface. For example, an increase in the work function indicates that electrons are shared with the adsorbate and are therefore harder to remove. Although no significant differences between the work functions of nickel and cobalt within an experimental accuracy of approximately 0.1 eV were observed, a large surface coverage dependence of the work function was reported for both metals. The large increases in the work function calculated are consistent with a typical picture of chemisorption of electronegative atomic adsorbates like carbon on transition metal surfaces. Electronegative adatoms typically form strong adatom–metal bonds and thereby remove the charge from the metal–metal bonds of the surface. Electronegative adsorbates such as carbon typically have a negative interaction energy with other adsorbates, which is manifested as a change in the binding energy as a function of surface coverage. In all cases of carbon chemisorption on nickel and cobalt studied, there was an increase in the charge inside the carbon muffin-tin sphere upon chemisorption. Although the charge differences between the two metal surfaces were negligible, the spatial location of this charge, as shown by both the DOS plots and the density difference plots, did vary. This variation was even more pronounced for a given metal surface as the surface coverage was altered.

These changes in the work function and the changes in the surface relaxation discussed earlier can be combined with the information provided by the density of states plots to provide a consistent picture of the nature of the bonding between carbon and nickel as the surface coverage is changed. The broad C(2s) band observed at higher surface coverages indicates that the bonding of carbon to the Ni(111) surface does not consist of individual, well-isolated C-Ni bonds, but rather that the carbon-induced states are delocalized over the whole surface plane and form a surface band. The formation of this carbon surface band was observed down to coverages of 0.5 ML. However, at the low coverage limit, $\Theta = 0.25$, the character of the C-Ni bonding is qualitatively different. The carbon surface band is no longer present, and the carbon–nickel bonding is comprised of states localized between the carbon and the nearest-neighbor nickel atoms.

The dependence of the binding energy on the surface coverage can be further rationalized in terms of the density of states and the density difference plots. At 1-ML coverage for both cobalt and nickel, the nonbonding dangling $C(2p_z)$ orbital was directed away from the surface and may contribute to a coulombic repulsion between neighboring carbon atoms, since it is less likely to be screened by the $4s + p$ delocalized electrons characteristic of a transition metal surface. A similar behavior was observed by Feibelman (38, 39) for carbon-covered Ru(0001) and Rh(111) surfaces. The density of states at the Fermi level determines the height over which perturbations of the charge density are screened. As seen from the DOS plots for 1-ML coverage, the DOS at the Fermi level is severely reduced and thus attenuates the effective screening length. Examination of these plots also provides insight into the energetic differences between Co(0001) and Ni(111) as the surface

coverage was varied. In Ni(111), the dangling nonbonding C($2p_z$) orbital has a higher occupation than it does in Co(0001). This higher occupancy increases the charge in this orbital, leading to a stronger coulombic repulsion and thus a decrease in the binding energy at a particular surface coverage.

The variation in the energetics and the electronic changes observed on Ni(111) and Co(0001) surfaces combine to form a qualitatively consistent picture of their reactivity differences. As the surface coverage was increased on both the Ni(111) and Co(0001) surfaces, the carbon hybridization shifted from sp^3 to sp^2, partially due to the formation of the nonbonding dangling C($2p_z$) orbital. This change in hybridization and the corresponding decrease in chemisorption energy lead to an increase in reactivity of the carbon atoms. Since the change in the binding energy as the surface coverage varied was more pronounced on nickel than on cobalt, it is expected that carbon on nickel would be more reactive than on cobalt. Indeed, this is observed experimentally by Vannice (40), where the turnover frequency over nickel was 60% greater than over cobalt.

One of the most interesting comparisons to emerge from the calculations reported in this work of carbon adsorbed on nickel and cobalt is the relative stability of the subsurface and surface sites and the change in the relative values with surface coverage. As the coverage decreased, the binding energies of the most stable surface site and the subsurface site approached one another. It is possible, therefore, that at a certain coverage, the binding energies would be equal, allowing for facile exchange between surface and subsurface sites as observed by Lauderback *et al.* (41) for carbon chemisorbed on a Ru(0001) surface.

The presence of surface carbon, subsurface carbon, and graphitic structures in different temperature regimes suggests relative values of the activation energies for their formation. Specifically, the high temperature required for carbon migration to form graphite suggests that the energy barrier is higher than that for movement of the carbon atoms into the subsurface which is observed to occur at lower temperatures. Studies by Massaro *et al.* (42) found that the activation energy for bulk diffusion for temperatures less than 973 K was $\simeq$20 kcal/mol. Our calculations suggest that in the low coverage limit the barrier for carbon migration is $\geq$21 kcal/mol. Assuming that the transformation from carbon at low coverage to a graphite structure proceeds through occupation of the most energetically favorable sites, the barrier for carbon–carbon bond formation can also be estimated from our calculations. The surface coverage dependence of the binding energy for these sites is plotted for both nickel and cobalt in Fig. 7 and suggests that the barrier is $\geq$39 kcal/mol over Ni(111) and 36 kcal/mol over Co(0001). These differences may also explain the greater tendency of cobalt to form higher molecular weight products during FT synthesis, while nickel is predominantly a methanation catalyst. In addition, the binding energy differences between the most stable threefold hollow site and the bridge site could provide insight into the energetic requirement for carbon–metal bond cleavage which has been linked to the hydrogenation rate of the catalyst (6). Over Ni(111), the values of ΔE_b (fcc hollow-bridge) are 15.9 kcal/mol and 7.4 kcal/mol for $\Theta = 0.25$ and 1.0, respectively. Likewise for Co(0001), the values of ΔE_b (hcp hollow-bridge) are 19.4 kcal/mol and 9.7 kcal/mol. These values suggest that hydrogenation is more energetically favored over Ni(111) than over Co(0001). Combining these results with the estimations of the carbon–carbon bond formation barrier reported above, it can be concluded that both the metal–carbon bond strength and the barrier for carbon–carbon bond formation are dependent on the valence–electron occupation.

Deactivation phenomena through the formation of a graphite overlayer may also be interpreted in terms of these energetic differences. Correlating activation energies with differences in the energy of stable configurations suggests that, since carbon is more strongly bound on cobalt as an isolated atom than it is on nickel, the energy barrier for transformation of monolayer graphite to isolated atoms is lower on cobalt than it is on nickel. This implies that the formation of graphite over nickel will more likely cause deactivation of the surface due to coverage of a chemically inactive graphite layer.

6. CONCLUSION

The calculations carried out in this work significantly expand the database of geometric and energetic parameters describing carbon adsorption on nickel and cobalt single crystal surfaces. Most importantly, the dependence of the binding energy on the adsorption site and the surface coverage was quantified, facilitated by the periodic nature of the FP-LAPW calculations carried out. For the small number of possible comparisons between our results and experimental values, good agreement was obtained. The most stable configuration for carbon was adsorption in the fcc threefold hollow on nickel and the hcp threefold hollow on cobalt at all surface coverages, but the relative stabilities were a pronounced function of surface coverage. At a particular adsorption site, the binding energy was a function of surface coverage, varying by 1.71 eV over nickel and 1.56 eV over cobalt, with a maximum value observed at 0.25-ML coverage. The results obtained suggest that both the metal–carbon bond strength and the barrier for carbon–carbon bond formation are dependent on the valence–electron occupation and surface coverage. The formation of a graphite overlayer was described in terms of a number of processes, including the dissolution of carbon into the subsurface and carbon deposition. The energetic values suggest that, if a graphite layer is formed, the process is irreversible due to

the high energetic barrier for carbon dispersion on the surface, with a higher energy barrier calculated for nickel than for cobalt. These energy maps obtained for these two surfaces provide insight into the relative tendency of cobalt and nickel toward higher hydrocarbon formation.

REFERENCES

1. Dumesic, J. A., Rudd, D. F., Aparicio, L. M., Rekoske, J. E., and Treviño, A. A., "The Microkinetics of Heterogeneous Catalysis." Am. Chem. Soc., Washington, DC, 1993.
2. Benziger, J. B., *in* "Metal-Surface Reaction Energetics" (E. Shustorovich, Ed.), Chap. 2, p. 53. VCH, New York, 1991.
3. Perdew, J., Burke, K., and Ernzerhof, M., *Phys. Rev. Lett.* **77**(18), 3865 (1996).
4. Blaha, P., Schwarz, K., Dufek, P., and Augustyn, R., "WIEN95: A Full Potential Linearized Augmented Plane Wave Package for Calculating Crystal Properties." Technical University Vienna, Austria, 1995.
5. Kohler, B., Wilke, S., Scheffler, M., Kouba, R., and Ambrosch-Draxl, C., *Comput. Phys. Commun.* **94**, 31 (1996).
6. van Santen, R. A., de Koster, A., and Koerts, T., *Catal. Lett.* **7**, 1 (1990). SE-11.
7. Goodman, D., Kelley, R., Madey, T., and White, J., *J. Catal.* **64**, 479 (1980).
8. Kelley, R., and Goodman, D., *Surf. Sci.* **123**, L743 (1982).
9. Goodman, D., *Acc. Chem. Res.* **17**, 194 (1984).
10. Goodman, D., and Houston, J., *Science* **236**, 403 (1987).
11. Shelton, J., Patil, H., and Blakely, J., *Surf. Sci.* **43**, 493 (1974).
12. Isett, L., and Blakely, J., *Surf. Sci.* **47**, 645 (1975).
13. Isett, L., and Blakely, J., *Surf. Sci.* **58**, 397 (1976).
14. Eizenberg, M., and Blakely, J., *Surf. Sci.* **82**, 228 (1979).
15. Mijoule, C., Baba, M. F., and Russier, V., *J. Mol. Catal.* **83**, 367 (1993).
16. Weinberg, W., and Merrill, R., *Surf. Sci.* **33**, 493 (1972).
17. Weinberg, W., and Merrill, R., *Surf. Sci.* **39**, 206 (1973).
18. Darling, G. R., Pendry, J. B., and Joyner, R. W., *Surf. Sci.* **221**, 69 (1989).
19. Jacobsen, K., and Nørskov, J. K., *Surf. Sci.* **166**, 539 (1986).
20. Mlynarski, P., and Salahub, D., *J. Chem. Phys.* **95**(8), 6050 (1991).
21. Swang, O., Faegri, K., Jr., Gropen, O., and Wahlgren, U., *Int. J. Quantum Chem.* **57**, 105 (1996).
22. de Koster, A., and van Santen, R. A., *J. Catal.* **127**, 141 (1991).
23. Burghgraef, H., Jansen, A. P. J., and van Santen, R. A., *Surf. Sci.* **324**, 345 (1995).
24. Joyner, R. W., Darling, G. R., and Pendry, J. B., *Surf. Sci.* **205**, 513 (1988).
25. Barbier, A., Pereira, E. B., and Martin, G., *Catal. Lett.* **45**, 221 (1997).
26. Zonnevylle, M., Geerlings, J., and van Santen, R., *Surf. Sci.* **240**, 253 (1990).
27. Klink, C., Stensgaard, I., Besenbacher, F., and Lægsgaard, E., *Surf. Sci.* **342**, 250 (1995).
28. Hoffmann, R., *Rev. Mod. Phys.* **60**(3), 601 (1988).
29. Cohen, M., Ganduglia-Pirovano, M., and Kudrnovský, J., *Phys. Rev. Lett.* **72**(20), 3222 (1994).
30. Villars, P., and Calvert, L., Eds., "Pearson's Handbook of Crystallographic Data for Intermetallic Phases," 2nd ed. ASM International, Materials Park, OH, 1991.
31. Lide, D. R. (Ed.), "CRC Handbook of Chemistry and Physics," 78th ed. CRC Press, New York, 1997.
32. Gamo, Y., Nagashima, A., Wakabayashi, M., Terai, M., and Oshima, C., *Surf. Sci.* **374**, 61 (1997).
33. Rosei, R., Modesti, S., Sette, F., Quaresima, C., Savoia, A., and Perfetti, P., *Phys. Rev. B* **29**(6), 3416 (1984).
34. Atrei, A., Bardi, U., Rovida, G., Torrini, M., Zanazzi, E., and Maglietta, M., *J. Vac. Sci. Technol. A* **5**(4), 1006 (1987).
35. Brodie, I., *Phys. Rev. B* **51**(19), 13660 (1995).
36. Banerjea, A., and Smith, J., *Phys. Rev. B* **37**(12), 6632 (1988).
37. Nagashima, A., Nuka, K., Satoh, K., Itoh, H., Ichinokawa, T., Oshima, C., and Otani, S., *Surf. Sci.* **287/288**, 609 (1993).
38. Feibelman, P., *Surf. Sci.* **103**, L149 (1981).
39. Feibelman, P., *Phys. Rev. B* **26**(10), 5347 (1982).
40. Vannice, M. A., *J. Catal.* **37**, 449 (1975).
41. Lauderback, L., and Delgass, W., *Surf. Sci.* **172**, 715 (1986).
42. Massaro, T. A., and Petersen, E. E., *J. Appl. Phys.* **42**(13), 5534 (1971).